ISBN: 978-3-95450-227-1 ISSN: 2673-5490 doi:10.18429/JACoW-IPAC2022-TUPOMS053

START-TO-END SIMULATIONS OF THE LCLS-II HE FREE ELECTRON LASER

D. Cesar*, G. Marcus, H.D. Nuhn, T. Raubenheimer, SLAC, Menlo Park, USA
J. Qiang, LBNL, Berkeley, USA

Abstract

In this proceeding we present start-to-end simulations of the LCLS-II-HE free electron laser. The HE project will extend the LCLS-II superconducting radio-frequency (SRF) linac from 4 GeV to 8 GeV in order to produce hard x-rays from the eponymous hard x-ray undulators (26 mm period). At the same time, soft x-ray performance is preserved (and extended into the tender regime) by using longer period undulators (56 mm period) than were originally built for LCLS-II (39 mm period). Here we use high-fidelity numerical particle simulations to study the performance of several SASE beamline configurations, and compare the resulting x-ray energy, power, duration, and transverse properties. Using the LCLS-II normal-conducting gun, we find that the x-ray pulse energy drops off rapidly above 15 keV, while using the lower emittance beam from a proposed SRF gun, we improve the cutoff to 20 keV.

LCLS-II HE

The next generation of free electron laser (FEL) facilities [1–3] is being built with superconducting radio-frequency (SRF) accelerators which can deliver beam at MHz repetition rates in order to simultaneously provide both high average and high peak power x-ray pulses. The LCLS-II HE project [4] plans to extend the operation of the LCLS-II facility from 4 GeV to 8 GeV by installing a new (SRF) linac downstream of the bunch compression and before the beam switchyard which delivers beam to the undulators. The SRF linac can be fed by two injectors: the LCLS-II very high frequency (VHF) injector; and a new (planned) superconducting, low emittance injector (LEI) [5, 6]. After being accelerated to 8 GeV the beam(s) can then be distributed to either hard or soft x-ray undulators, as shown in Fig. 1.

Doubling the beam energy will boost the resonant photon energy by a factor of four, allowing the 26 mm period hard x-ray undulators to produce first-harmonic photons out to 20 keV. At such small wavelengths 3D effects [7] greatly impact the gain length, and so the new low emittance injector is being designed to deliver (rms) emittances as low as 0.1 um. Simulations show that this lower emittance dramatically improves the yield above 15 keV and allows us to take full advantage of the 8 GeV beam.

At the same time, the existing 39 mm ($K_{max} \approx 5.4$) period LCLS-II soft x-ray undulators will be unable to produce photon energies below 1 keV when the electron beam energy is 8 GeV. In order to reach the often requested C (285 eV), N (400 eV), and O (532 eV) k-edges the HE project currently plans to replace the existing 39 mm period soft x-ray undulators with longer, 56 mm period undulators ($K_{max} \approx 9.2$) (rather than build a 4 GeV extraction line). Increasing the undulator period from 39 mm to 56 mm allows the 8 GeV beam to be resonant with lower photon energies, but it also increases the physical gain length. For fixed photon energy, beam current, emittance, and focusing lattice, the Pierce parameter, $\rho \propto \frac{1}{\gamma}\left(\frac{K\lambda_u}{\sigma_r}\right)^{2/3}$, increases by only 10% from 4 to 8 GeV, while the 1D gain length $L_g \propto \lambda_u/\rho$ increases by more than 30% [7]. The HE program plans to add extra undulator segments to make up the difference (one design under study is shown in Fig 1).

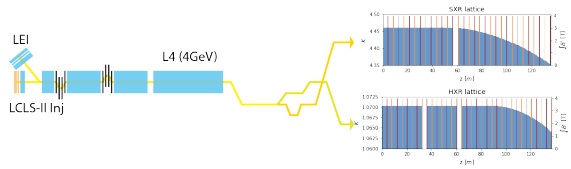

Figure 1: Cartoon of the LCLS-II HE facility (excluding the normal conducting, "copper" accelerator). Two injectors (the LCLS-II VHF gun and a new low emittance injector (LEI)) can feed an 8 GeV linac. A beam switchyard delivers these beams to the HXR line (bottom) or the SXR line (top).

START TO END SIMULATIONS

High fidelity numerical particle simulations have an established history of use for modeling and optimizing facility design. Here we use the IMPACT suite for the accelerator [8, 9], and then we use GENESIS [10] to model the FEL lasing process. The IMPACT codes include, where necessary, the effects of shot noise, 3D space charge, RF and resistive wall wakefields, coherent synchrotron radiation (CSR), and intra-beam scattering; while GENESIS models the FEL instability slice-wise, in the slowly varying envelope approximation. This approach has been benchmarked at LCLS [11] and was used extensively during the development of LCLS-II [12, 13].

Electron Beam

In Fig. 2 we show three sample electron beams delivered to the HXR undulator: 20 pC and 100 pC beams from the LCLS-II VHF injector, as well as a 100 pC beam from a low emittance injector. The (core) beam quality is summarized in Table 1. The low emittance injector has the best beam quality, while the 20 pC has the worst. However, the 20 pC beam still has use in reducing the average electron beam power and also creates for creating a shorter FEL pulse (20 fs vs 40 fs) that is less sensitive to 3D effects than the

* dcesar@slac.stanford.edu

Content from this work may be used under the terms of the CC BY 4.0 licence (© 2022). Any distribution of this work must maintain attribution to the author(s), title of the work, publisher, and DOI

ISBN: 978-3-95450-227-1 ISSN: 2673-5490 doi:10.18429/JACoW-IPAC2022-TUPOMS053

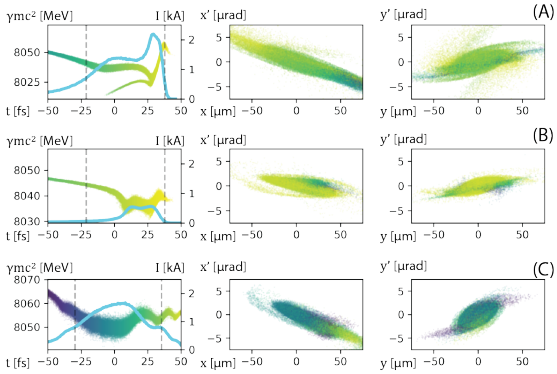

Figure 2: Example phase space of the LCLS-II HE scH (superconducting to hard) beam path from start-to-end simulations. (A) 100 pC from the LCLS-II injector (B) 20 pc from the LCLS-II injector (C) 100 pC from a lower emittance injector. The head is to the right (positive 'time').

comparable 100 pC beam. All three beams show slice-by-slice variation in the transverse beam parameters, due largely to CSR during bunch compression. To optimize the FEL process we match the beam core to the unudulator lattice rather than the projected beam.

FEL

The FEL is simulated by sampling the output of the IMPACT particle tracking and importing it into a realistic lattice in GENESIS which includes focusing, resistive wall wakefields, and interspace breaks (see Table 2). To reduce simulation time, only the portion of the beam between the dashed lines in Fig. 2(A) is imported into GENESIS (the "core" used for matching is only half of this extent). The complicated longitudinal-transverse correlations present in the electron beam are faithfully reproduced in GENESIS and become imprinted on the photon beam as a slice-dependent source size, position, and pointing.

The undulators are given an piece-wise linear (undulator-by-undulator) approximation to a quadratic taper ($K = K_0 + K_1 z + K_2 (z - z_0)^2 \Theta(z - z_0)$) whose parameters are chosen to maximize pulse energy. The linear rate K_1 is chosen to match the average energy loss in the beam core (due to wakefields and spontaneous undulator radiation), the quadratic rate K_2 is chosen by simplex optimization, and the starting point Z_0 by a greedy algorithm which assumes the starting point should be shortly before saturation and increasing with photon energy. By optimizing on pulse energy, we find a taper which is a compromise between tapering for the core electrons and the mismatched head and tail electrons.

For large K (low photon energy) the gain lengths of all three beams being studied are quite short (see Fig. 3), such that we must taper quite strongly (and differently for each beam). Due to diffraction, this can be challenging around the chicane breaks (see Fig 1, [14–16]), but it illustrates our capability to easily support two-color lasing.

For low K (high photon energy) the the gain lengths are much longer, and we see can see clearly the effect of reduced

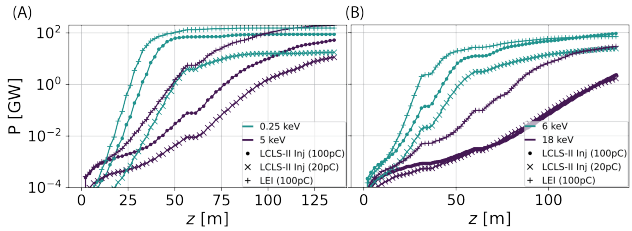

Figure 3: Gain profile for the three electron sources delivered to the soft (A) and hard (B) x-ray lines. The breaks correspond to the location of chicanes (which are turned off here). Notice how the gain of the LEI beam is significantly faster at high photon energy.

emittance. We see that the 20 pC typically produces lower peak power (due to its reduced beam power), but that in the 18 keV case it actually catches up to the 100 pC beam due to its reduced emittance. The performance boost for the LEI is even more dramatic, and it obviates the importance of high beam quality for producing these high energy photons.

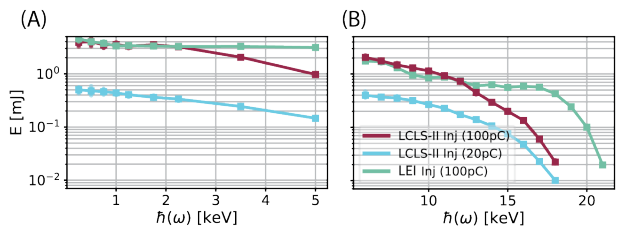

Figure 4: Pulse energy for the three electron sources delivered to the soft (A) and hard (B) x-ray lines. The high core brightness of the LEI beam allows it lase more efficiently at short wavelengths.

In Fig. 4 we summarize the saturated FEL pulse energy as a function of photon wavelength for the SXR and HXR lines. In all cases we see that the 20 pC beam produces the least energy, while the LEI produces the greatest. We can observe a general difference between the SXR and HXR, however, in that the SXR line is less sensitive to photon energy. This is because the HXR line runs out of unudlators in the exponential regime, while on the SXR line we have enough undulators to taper well past saturation (especially when driven by the LEI). The large number of undulators on the SXR line are needed to improve performance for more advanced modalities such as two-color x-ray generation and self-seeding [14, 15, 17].

The high-resolution numerical particle tracking simulations performed here allow us to realistically model the gain length and ultimately the electron-to-photon efficiency of the entire system. But beyond emphasizing the importance of core beam brightness, using the realistic beam in FEL simulations allows us to also accurately model the FEL source size and divergence, including complicated correlations originating from CSR in the electron beam. For example, in Fig. 5 we show the electron beam density (from the LCLS-II VHF injector) in the z-x (longitudinal-bend) plane near the end of

Content from this work may be used under the terms of the CC BY 4.0 licence (© 2022). Any distribution of this work must maintain attribution to the author(s), title of the work, publisher, and DOI

ISBN: 978-3-95450-227-1 ISSN: 2673-5490 doi:10.18429/JACoW-IPAC2022-TUPOMS053

Table 1: Core Beam Parameters. 100pC from LCLS-II VHF Unless Otherwise Labeled.

	HXR	HXR 20 pC	HXR LEI	SXR	SXR 20 pC	SXR LEI
I [kA]	1.35	0.52	1.65	1.35	0.52	1.65
ϵ_x [um] (rms)	0.25	0.18	0.13	0.27	0.19	0.14
ϵ_y [um] (rms)	0.28	0.17	0.13	0.28	0.17	0.13
$\Delta\gamma mc^2$ [MeV] (rms)	1.12	1.08	1.71	1.12	1.1	1.73

Table 2: Undulator Lattice Elements Used in This Study

	λ_u [cm]	N_u/cell [$\#\lambda_u$]	L_{cell} [$\#\lambda_u$]	$K_{\max}$	$\int B'dl$ [T]
HXR	26	130	155	>2.44	4
SXR	56	60	78	>9.21	4

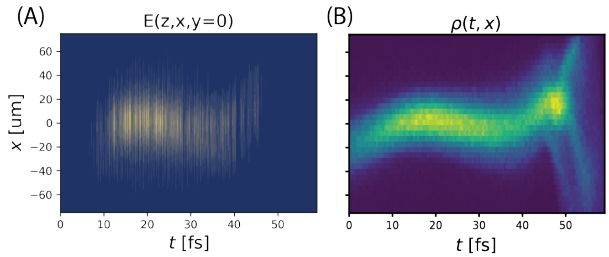

Figure 5: Longitudinal-transverse coupling in (A) the near field profile of a 16 keV x-ray beam and (B) the electron beam particle density (for 100pC beam from LCLS VHF injector). The correlations originate from CSR induced energy loss during compression of the electron beam.

the HXR undulator as compared to the near-field profile of 16 keV HXR photons. The snaking of the electron beam is faithfully replicated in the near-field profile, albeit with some blurring since we are nearing saturation and there is notable radiation from previous undulators (where, a betratron phase advance away, the electron profile is flipped). The effect is strongest in the near-field, but the model shows significant oscillation in the far-field as well.

In addition to these centroid oscillations, the photon beam undergoes some slice-by-slice variation in spot-size and divergence. But, since these have a weaker dependence on the electron beam parameters, they are most notable at the outer 10% where the electron beam is most mismatched. Overall the centroid oscillation is the biggest effect, leading to an increase in the projected etendue of the photon beam.

CONCLUSION

High resolution numerical particle simulations allow us to create a realistic model of the LCLS-II HE FEL beam. We use this model to validate and optimize the design of the accelerator and undulator beamlimes, as well as to estimate the ultimate performance of the FEL. Our simulations show that the soft x-ray line can achieve as much >0.4% electron-to-x-ray efficiency from 0.25 keV through the 5 keV tender range. The hard x-ray line achieves similar efficiency near 5 keV, but falls off rapidly as we run out of space to taper. Our simulations suggest that a new lower emittance injector would extend the HXR range out as far as 20 keV.

ACKNOWLEDGEMENTS

Thanks to Chris Adolphsen and Fuhao Ji, among others, for their work helping to model a low emittance injector for the HE project. This work is supported in part by DOE Contract No. DE-AC02-76SF00515.

REFERENCES

[1] J. N. Galayda, "The LCLS-II: A High Power Upgrade to the LCLS," in *Proc. IPAC'18*, Vancouver, Canada, Apr.-May 2018, pp. 18–23, doi:10.18429/JACoW-IPAC2018-MOYGB2

[2] W. Decking *et al.*, "A MHz-repetition-rate hard X-ray free-electron laser driven by a superconducting linear accelerator," en, 6, vol. 14, 2020, pp. 391–397, doi:10.1038/s41566-020-0607-z

[3] Z. Zhao, D. Wang, Z.-H. Yang, and L. Yin, "SCLF: An 8-GeV CW SCRF Linac-Based X-Ray FEL Facility in Shanghai," en, *Proceedings of the 38th Int. Free Electron Laser Conf.*, vol. FEL2017, pp. 182–184, 2018, doi:10.18429/JACOW-FEL2017-MOP055

[4] T. Raubenheimer, "The LCLS-II-HE, A High Energy Upgrade of the LCLS-II," en, *Proceedings of the 60th ICFA Advanced Beam Dynamics Workshop on Future Light Sources*, vol. FLS2018, pp. 6–11, 2018, doi:10.18429/JACOW-FLS2018-MOP1WA02

[5] J. Qiang, T. Raubenheimer, and M. Woodley, "Beam Dynamics Optimization of LCLS-II HE Linear Accelerator Design," en, *Proceedings of the 12th International Particle Accelerator Conference*, vol. IPAC2021, pp. 3224–3227, 2021, doi:10.18429/JACOW-IPAC2021-WEPAB251

[6] "LCLS-II-HE Low Emittance Injector Conceptual Design Report," Tech. Rep. LCLSIIHE-1.1-DR-0418-R0, 2022.

[7] Z. Huang and K.-J. Kim, "Review of x-ray free-electron laser theory," *Physical Review Special Topics - Accelerators and Beams*, vol. 10, no. 3, p. 034801, 2007, doi:10.1103/PhysRevSTAB.10.034801

[8] J. Qiang, R. D. Ryne, S. Habib, and V. Decyk, "An object-oriented parallel particle-in-cell code for beam dynamics simulation in linear accelerators," *Journal of Computational Physics*, vol. 163, no. 2, pp. 434–451, 2000.

Content from this work may be used under the terms of the CC BY 4.0 licence (© 2022). Any distribution of this work must maintain attribution to the author(s), title of the work, publisher, and DOI

ISBN: 978-3-95450-227-1 ISSN: 2673-5490 doi:10.18429/JACoW-IPAC2022-TUPOMS053

[9] J. Qiang, R. D. Ryne, M. Venturini, A. A. Zholents, and I. V. Pogorelov, "High resolution simulation of beam dynamics in electron linacs for x-ray free electron lasers," *Physical Review Special Topics - Accelerators and Beams*, vol. 12, no. 10, p. 100702, 2009, doi:10.1103/PhysRevSTAB.12.100702

[10] S. Reiche, "GENESIS 1.3: A fully 3D time-dependent FEL simulation code," en, *Nuclear Instruments and Methods in Physics Research Section A: Accelerators, Spectrometers, Detectors and Associated Equipment*, vol. 429, no. 1, pp. 243–248, 1999, doi:10.1016/S0168-9002(99)00114-X

[11] J. Qiang *et al.*, "Start-to-end simulation of the shot-noise driven microbunching instability experiment at the Linac Coherent Light Source," *Physical Review Accelerators and Beams*, vol. 20, no. 5, p. 054402, 2017, doi:10.1103/PhysRevAccelBeams.20.054402

[12] G. Marcus *et al.*, "High Fidelity Start-to-end Numerical Particle Simulations and Performance Studies for LCLS-II," in *Proc. FEL'15*, Daejeon, Korea, Aug. 2015, pp. 342–346, doi:10.18429/JACoW-FEL2015-TUP007

[13] J. Qiang *et al.*, "Start-to-End Simulation of the LCLS-II Beam Delivery System with Real Number of Electrons," in *Proc. FEL'15*, Daejeon, Korea, Aug. 2015, pp. 714–717, doi:10.18429/JACoW-FEL2015-WEP070

[14] E. Hemsing *et al.*, "Soft x-ray seeding studies for the SLAC Linac Coherent Light Source II," *Physical Review Accelerators and Beams*, vol. 22, no. 11, p. 110701, 2019, doi:10.1103/PhysRevAccelBeams.22.110701

[15] C. Yang *et al.*, "Self Seeding Scheme for LCLS-II-HE," en, *Proceedings of the 9th Int. Particle Accelerator Conf.*, vol. IPAC2018, pp. 4414–4417, 2018, doi:10.18429/JACOW-IPAC2018-THPMK055

[16] G. Marcus and F.-J. Decker, "Cavity-based x-ray free-electron laser research and development," en, *39th Free Electron Laser Conf./ FEL2019, Hamburg, Germany*, pp. 282–287, 2019, doi:10.18429/JACoW-FEL2019-TUD04

[17] A. A. Lutman *et al.*, "Fresh-slice multicolour X-ray free-electron lasers," en, *Nature Photonics*, vol. 10, no. 11, pp. 745–750, 2016, doi:10.1038/nphoton.2016.201

Content from this work may be used under the terms of the CC BY 4.0 licence (© 2022). Any distribution of this work must maintain attribution to the author(s), title of the work, publisher, and DOI